energies

MDPI

Article

Active Thermal Management Method for Improving Current Capability of Power Devices under Influence of Random Convection

Weichao He [1], Yiming Zhu [1,*], Zijian Liu [1], Zhanfeng Ying [1,*] and Wei Zu [2]

[1] School of Energy and Power Engineering, Nanjing University of Science and Technology, Nanjing 210094, China; heweichao@njust.edu.cn (W.H.); zjliu@njust.edu.cn (Z.L.)
[2] National Key Laboratory of Transient Physics, Nanjing University of Science and Technology, Nanjing 210094, China; 222121010109@njust.edu.cn
* Correspondence: ymzhu@njust.edu.cn (Y.Z.); zhanfengying@njust.edu.cn (Z.Y.)

Abstract: The active thermal management (ATM) method can improve the current capability of power devices safely by utilizing the thermal limit of the device. However, the existing methods are not suitable for power devices affected by random convection. This is because the randomness of convection will lead to the uncertainty of increased current capability, which is unacceptable in most engineering applications. To overcome the shortcomings of existing ATM methods, this paper proposed a novel ATM method for power devices under the influence of random convection. In the proposed method, the short-time current capability of the power device is maximized according to the thermal inertia of the device and maximum load current. The continuous current capability of the power device is determined by a maximum continuous current that satisfies the over-temperature risk constraint of the device. To accurately estimate the maximum continuous current, an uncertainty model is presented for the convective thermal resistance of the power device based on wavelet packet transform and Markov chain. A series of experimental studies are carried out by taking a power MOSFET as an example. The experimental results show that the proposed method can safely improve the output performance of the power device without causing random fluctuations in the current capability.

Keywords: active thermal management; natural air-cooled; power converters; wavelet packet transform; Markov chain

check for updates

Citation: He, W.; Zhu, Y.; Liu, Z.; Ying, Z.; Zu, W. Active Thermal Management Method for Improving Current Capability of Power Devices under Influence of Random Convection. *Energies* **2024**, *17*, 3249. https://doi.org/10.3390/en17133249

Academic Editor: Christopher Micallef

Received: 8 May 2024
Revised: 28 June 2024
Accepted: 28 June 2024
Published: 2 July 2024

Copyright: © 2024 by the authors. Licensee MDPI, Basel, Switzerland. This article is an open access article distributed under the terms and conditions of the Creative Commons Attribution (CC BY) license (https://creativecommons.org/licenses/by/4.0/).

1. Introduction

As an important component of power converters, power devices have been widely applied in many fields, such as power systems, industrial manufacturing and electric vehicles [1,2]. With the increasing complexity of application scenarios and operating conditions, converters often need to be overloaded, which puts forward higher requirements for the current capability of power devices. Since increasing the current will lead to an increase in the device junction temperature, how to increase the output current of the device as much as possible without affecting thermal safety has always been a hot issue in engineering.

The most direct way to increase the device's current capability is to adopt a conservative thermal design. The basic idea of conservative thermal design is to provide a sufficient thermal safety margin for the device through some measures, such as adding additional cooling equipment, increasing cooling power and paralleling multiple devices, etc. [3,4]. Obviously, the conservative thermal design inevitably increases the volume, mass or cost of the cooling system, reducing the economy and competitiveness of the power converter.

In order to reduce the conservation of thermal design, the active thermal management (ATM) method of power devices has been proposed and developed rapidly in recent years [5,6]. The basic principle of the ATM method is to control the maximum junction temperature or junction temperature change trajectory of the power device by some means of actively manipulating the device loss, including adjusting the working current limit [7,8],

switching frequency [9,10], gate resistance [11] and modulation strategy [12], etc. The change trajectory control of the junction temperature helps to smooth the thermal stress fluctuation of the device and prolong the lifetime of the converter, while the maximum junction temperature control can be used to avoid the thermal breakdown of the device and improve the thermal safety of the converter. If the maximum junction temperature is controlled by changing the working current limit, the active thermal management method can maximize the device's current capability by utilizing the thermal limit of the device and then improving the loading capacity of converters.

The effect of the ATM method on improving the current capability of the power device can be analyzed in two stages. Before the power device reaches its thermal limit, the ATM method maximizes the short-time current capability of the device according to the thermal inertia of the device. When the device reaches the thermal limit state, the ATM method maximizes the continuous current capability of the device by controlling the device junction temperature. Therefore, the ATM method can improve the device's current capability without changing the existing cooling method and heat dissipation cost of converters. This is an advantage that other thermal management methods cannot match.

With this advantage, the ATM method has been applied to various power devices and converters. In [5,7], the ATM method is used to reliably improve the performance limit of power modules, thereby improving the utilization of the module. Ref. [13] proposes an ATM method for power devices to achieve optimal and low-cost design of power electronic systems. In [14,15], the ATM method is combined into the vector control strategy of the motor driver, so that the motor can safely increase the torque limit. An ATM method is proposed in [16] to ensure the device life and loading capacity of the photovoltaic converter under thermal limit. These scientific research and engineering applications have proved that the ATM method is an efficient and low-cost method for mining the potential output performance of power devices.

However, in the existing studies, power devices commonly work in a stable or determined working environment. With the continuous expansion of application scenarios, more and more power devices are used in natural air-cooled converters, including portable DC power supplies, movable inverters, photovoltaic controllers, etc. The devices in these converters are tightly attached to the inner wall of the converter enclosure and the enclosure is used as the heatsink for the device heat dissipation. Consequently, the heat dissipation capacity of the devices is dependent on the convection conditions in the converter working environment. It is well known that the natural airflow is unstable in most cases, which leads to the uncertainty of convective heat dissipation. Therefore, the power devices in the natural air-cooled converter will be affected by the random convection.

For the existing ATM method, the random convection is the uncertain disturbance that will cause random fluctuations in the increased device current capability and lead to the unstable overload capacity of the converter. This is not allowed in most engineering applications. For example, the uncertain overload capacity of the power supply will reduce the unreliability of load management strategies and the security of load operation. The random overload capability of the motor driver affects the stability of the peak torque, resulting in serious mechanical vibration and noise. Therefore, the existing ATM methods are not suitable for improving the current capacity of power devices under the influence of random convection.

To address this issue, this paper proposes a novel ATM method for power devices. This method maximizes the short-time current capability of the device according to the thermal inertia of the device and maximum allowable load current. The continuous current capability of the device is determined by a maximum continuous current that satisfies the over-temperature risk constraint of the device under random convection conditions. Based on wavelet packet transform and Markov chain, an uncertainty model is presented for the convective thermal resistance of the power device and is used to assess the maximum continuous current. Taking a single-power MOSFET as the object, the effectiveness and advantages of the proposed method are verified by experimental results.

2. Shortcomings of Applying Traditional ATM Method to Power Devices under Random Convection Conditions

2.1. Traditional ATM Method for Improving Current Capability of Power Devices

Manipulating the working current limit is the simplest ATM method to control the junction temperature of power devices, and it is also the most essential method to improve the device's current capability. For a single power device, the block diagram of the ATM method based on the working current limit manipulating is shown in Figure 1.

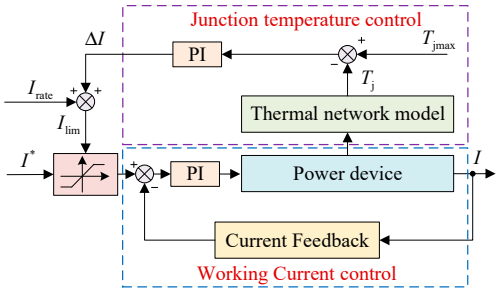


Figure 1. Block diagram of ATM method based on the working current limit manipulating.

There are two kinds of closed-loops in the ATM method, one for device working current I control and other for device junction temperature T_j control. T_{jmax} is the maximum allowable junction temperature and is used as a reference of the junction temperature control. The output of the junction temperature controller is a current variation ΔI. A current limit I_{lim}, which is the sum of ΔI and the rated current I_{rate}, is used to limit the device's working current. The rated current I_{rate} is a long-term working current measured under the rated environmental conditions of the power device.

Due to the fact that the junction temperature controller can prevent the device from over-temperature, I_{lim} represents the maximum current that the power device can safely output under present environmental conditions. With the protection of this current limit, the current expectation I^* in the current control can be greatly improved to enhance the device's current capability.

It should be noted that the device current cannot be increased indefinitely, otherwise the connected loads will be damaged. Therefore, I_{lim} should not exceed a maximum load current $I_{maxload}$ that is determined by the performance of loads.

2.2. Thermal Network Model of Power Devices

The junction temperature of power devices is commonly estimated by the thermal network model because it is difficult to measure directly in practical engineering [17,18]. Since this paper takes a power MOSFET as the research object, Figure 2 shows the typical junction-to-environment thermal network model of the power MOSFET. This model is composed of an RC thermal network from the junction to the case and an RC thermal network from the case to the environment, as shown in Figure 2.

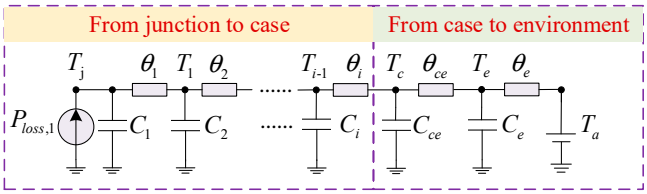


Figure 2. Junction-ambient thermal network model for a power MOSFET with a heatsink.

In the above thermal network model, T, C and θ are common symbols representing temperature, heat capacity and thermal resistance, respectively [19]. The parameters T_i, C_i and θ_i represent the temperature, the thermal capacity and the thermal resistance of

node i in the device, respectively. C_{ce} and θ_{ce} are, respectively, the thermal capacity and the thermal resistance of the thermal conductive material between the device and the heatsink. P_{loss}, T_c and T_a are the power loss, the case temperature and the ambient temperature, respectively. C_e and T_e are the thermal capacity and the temperature of the heatsink, respectively. θ_e is the thermal resistance between the heatsink and the environment. Since this thermal resistance characterizes the effect of environmental convection on the case temperature and the junction temperature, it is also called convective thermal resistance.

The thermal network from junction to case is expressed as

$$\begin{cases} C_1 \dfrac{dT_j}{dt} = P_{loss} - \dfrac{T_j - T_1}{\theta_1} \\ C_2 \dfrac{dT_1}{dt} = \dfrac{T_j - T_1}{\theta_1} - \dfrac{T_1 - T_2}{\theta_2} \\ \cdots\cdots \\ C_i \dfrac{dT_{i-1}}{dt} = \dfrac{T_{i-2} - T_{i-1}}{\theta_{i-1}} - \dfrac{T_{i-1} - T_c}{\theta_i} \end{cases} \tag{1}$$

The thermal network from case to ambient environment is given as

$$\begin{cases} C_{ce} \dfrac{dT_c}{dt} = \dfrac{T_{i-1} - T_c}{\theta_i} - \dfrac{T_c - T_e}{\theta_{ce}} \\ C_e \dfrac{dT_e}{dt} = \dfrac{T_c - T_e}{\theta_{ce}} - \dfrac{T_e - T_a}{\theta_e} \end{cases} \tag{2}$$

The parameters in (1), such as the losses, the thermal resistances and heat capacities, can be determined with the datasheet parameters provided by the manufacturers [15,20]. Although the thermal parameters in the datasheet ignore the temperature dependence of the material (especially for the thermal parameters of power MOSFETs), they are still widely used due to their convenience. In most cases, the accuracy of the thermal parameters provided by the manufacturer is considered to be able to basically meet the actual engineering needs.

The thermal parameters in (2) can be calculated with the physical definition of thermal resistance and thermal capacity, which are given by

$$\theta_{ce} = \frac{d_{ce}}{\lambda A_{ce}} \tag{3}$$

$$C_{ce} = c_{ce} m_{ce} \tag{4}$$

$$C_e = c_e m_e \tag{5}$$

where λ, d_{ce} and A_{ce} are the thermal conductivity, thickness and area of the thermal conductive tape between the case and heatsink, respectively. c_{ce} and c_e are the specific heat capacity of thermal conductive tape and heatsink, respectively. m_{ce} and m_e are the mass of thermal conductive tape and heatsink, respectively. Among these parameters, A_{ce}, d_{ce}, m_{ce}, and m_e can be measured by slide gauges and electronic scales. The parameters λ, c_{ce} and c_e can be found in the specifications provided by the manufacturer.

When the case temperature T_c is measured in real-time, the junction temperature T_j can be obtained only by (1). If the ambient temperature T_a is used as the boundary temperature, the junction temperature T_j should be estimated simultaneously by (1) and (2).

2.3. Experiment Set-Up

An experimental platform, as shown in Figure 3, is set up to analyze the shortcomings of the traditional ATM method in improving the current capacity of the power device under random convection conditions.

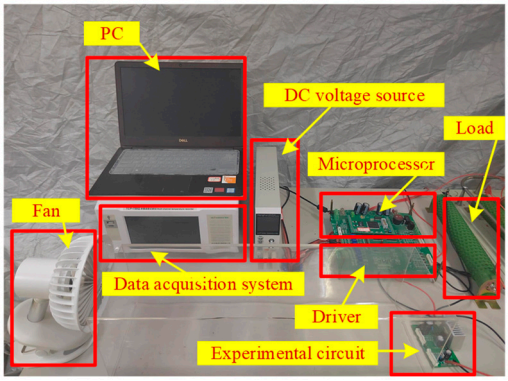


Figure 3. Picture of the experimental platform.

In this platform, a power MOSFET with a type of IRFB4410PbF (Infineon, Shenzhen, China) is employed as the experimental object and it is attached to a heatsink through the thermal conductive adhesive tape TR6400. The tape is a solid tape, which ensures that the thickness of the thermally conductive material between the device and the heatsink is constant. The structure and size of the heatsink are shown in Figure 4. Table 1 lists the material parameters of thermal conductive adhesive tape and heatsink. According to Table 1 and the datasheet of the manufacturer, and Table 2 lists the main thermal parameters in the junction-ambient thermal network model of the power MOSFET.

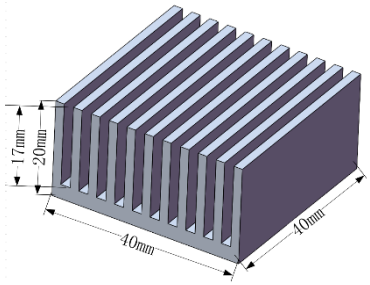


Figure 4. Structure and size of the heatsink.

Table 1. Material parameters of thermal conductive adhesive tape and heatsink.

Parameters	λ (W/m/k)	d_{ce} (mm)	A_{ce} (cm^2)	c_{ce} (J/g/°C)	c_e (J/g/°C)	m_{ce} (mg)	m_e (g)
values	0.8	0.2	3.32	0.92	0.88	11	7.35

Table 2. Main thermal parameters in the junction-ambient thermal network model.

Thermal Resistance (°C/W)			Heat Capacity (J/°C)			
θ_1	θ_2	θ_{ce}	C_1	C_2	C_{ce}	C_e
0.2736	0.3376	0.7530	0.0014	0.0123	0.0105	6.4550

The power MOSFET is connected in a simple experimental circuit, as shown in Figure 5. In this circuit, a 0.5ohm resistor is connected to the drain of the power MOSFET as the loads. A DC voltage source of 18 V is employed to supply power to the circuit. A controller provides a PWM signal to a driver to control the device's working current. This controller is designed based on microprocessor RK3586 (Rockchip, Fuzhou, China) whose main frequency is 1.8 GHz/4 cores and memory is 2 GB.

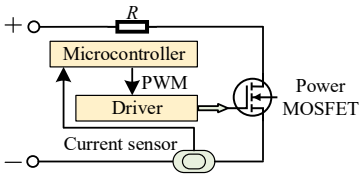


Figure 5. Experimental circuit of the power MOSFET.

An electric fan with controllable speed is utilized to simulate the random variations if airflow in the environment. Since the experimental circuit is not equipped with an enclosure, the power device is directly exposed to the convection environment. This is conducive to the study of the ATM method under strong random convection conditions. To effectively reflect the thermal dynamic characteristics of the experimental object, the K-type thermocouples with a thermal response time of 0.5 s are used to measure the heatsink and ambient temperature. All of the measurement data is collected by a data acquisition system with a period of 1 s and sent to a PC for storage and analysis.

To provide a sufficient thermal safety margin for the device in the experiment, the maximum allowable junction temperature T_{jmax} in this study is limited to 85 °C. The rated working current I_{rate} of the power device is 0.6 A, which is determined in a conservative environment without forced convection and with an ambient temperature of 40 °C. The maximum load current $I_{maxload}$ of the power device is 1.2 times the rated current, which is determined according to the maximum power rating of the load resistor. The ambient temperature T_a during the experiment is maintained at 20 °C, which creates favorable environmental conditions to improve the device's current capability.

2.4. Analysis of Shortcomings of the Traditional ATM Method

To analyze the shortcomings of the traditional ATM method, two experiments are carried out under stable and random convection conditions, respectively. Both experiments lasts 180 min and each of them is equally separated into two time periods, I and II. During these two time periods, the power device works with the rated current and the ATM method, respectively. The expected working current I^* in the ATM method is set to the maximum load current $I_{maxload}$.

The variations if the device junction temperature and the working current in the stable convection environment are shown in Figure 6. The airflow rate in this experiment is stably controlled at 0.35 m/s by the electric fan. The working current I is expressed as the normalized current whose reference value is the rated current I_{rate}. The normalized current can more conveniently reflect the current capacity of the device increased by the ATM method.

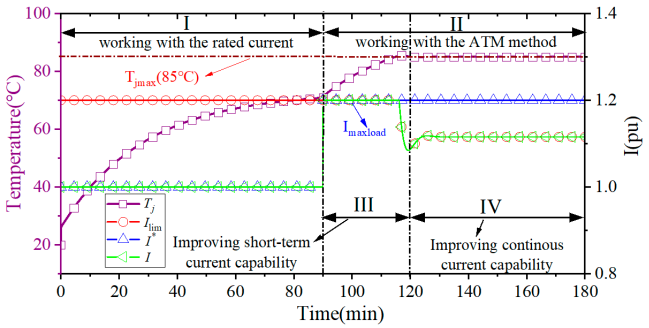


Figure 6. Variations if the device junction temperature and the working current in the stable convection environment.

From period I, it can be found that the device junction temperature T_j under the rated current continues to rise and then reaches a steady state. In period II, the device junction

temperature is gradually controlled to the maximum allowable temperature T_{jmax} by the ATM method and the device working current I is obviously increased during this period.

The performance of the ATM method can be analyzed in period III and period IV, which are separated from period II. During period III, the junction temperature T_j has not yet reached T_{jmax} due to the thermal inertia of the power device. Consequently, the ATM method increases the current limit I_{lim} to the maximum load current $I_{maxload}$ based on the junction temperature control. This means that the device can work for a short time at 1.2 times the rated current. In period IV, the ATM method decreases the current limit I_{lim} to 1.18 pu to control the junction temperature at T_{jmax}. Since the device has reached its thermal limit, the current of 1.18 pu represents the maximum current that the device can continue to work under given environmental conditions. Although the current limit of this time period is lower than that of period III, it is still higher than the rated current. Therefore, the ATM method is able to safely improve the short-term and continuous current capability of the power device under stable convection conditions.

Next, let us analyze the experiment of the device working under random convection conditions. To generate real airflow changes in the experimental environment, a set of random airflow rate data was collected in the outdoor environment with a sampling period of 1 s. Figure 7 compares the real airflow rate and the airflow rate generated by the fan. The full-scale deviation between the two airflow rates is less than 8.7%F.S., indicating that the airflow generated in the experimental platform effectively reflects the randomness of convection in the natural environment.

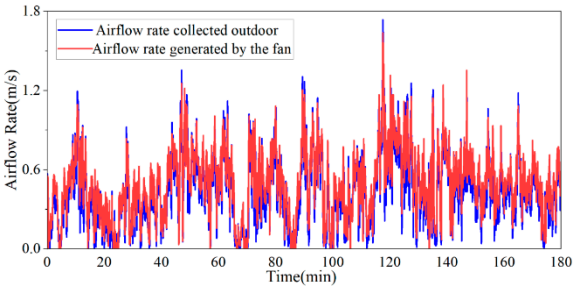


Figure 7. Comparison of airflow rates collected outdoor and generated by fan.

Figure 8 shows the variations in the device junction temperature and the working current in the random convection environment. Compared with period III in Figure 6, it can be found that the random convection does not affect the short-term current capacity of the device improved by the ATM method. The reason is that before the junction temperature reaches T_{jmax}, the power device working with the maximum load current $I_{maxload}$ does not generate the risk of over-temperature. However, I_{lim} fluctuates significantly in period IV, because the ATM method has to compensate the disturbance of random convection to the junction temperature control by changing the current limit. It can be found that the maximum current fluctuation reaches about 0.04 pu, which is 4% of the rated current. Although the fluctuation is not severe in this paper, it does lead to overload instability for converters. As mentioned before, this is unacceptable in most practical projects and urgently needs improvement. Furthermore, if the airflow rate in the convective environment is increased or the heat capacity of the heatsink is reduced, the current capacity fluctuation will further increase. Therefore, it is necessary to avoid the fluctuation of current capacity caused by the ATM method in a random convection environment.

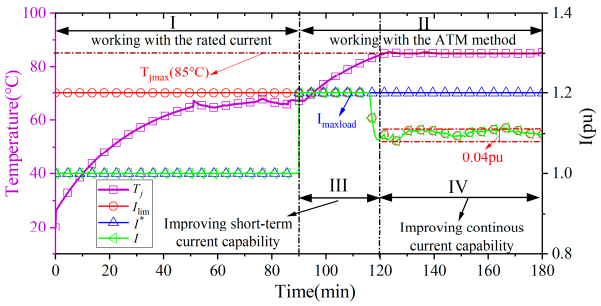


Figure 8. Variations if the device junction temperature and the working current in the random convection environment.

3. Uncertainty Model of Convective Thermal Resistance for Power Devices under Random Convection Conditions

3.1. Extraction of Convective Thermal Resistance Samples

According to heat transfer theory [21], the influence of convection on the heat dissipation capacity of the device can be characterized by the convective thermal resistance between the device and the ambient environment. The random variation in ambient air velocity will lead to the uncertainty of the convective thermal resistance of devices. In order to improve the active thermal management method, it is necessary to establish an uncertainty model of the convective thermal resistance.

The primary condition for establishing an uncertainty model is to obtain random samples. The convective thermal resistance of the device is affected by many nonlinear factors such as air density, dynamic viscosity and so on. The above-influencing factors are uncertain and difficult to estimate in real time under random convection conditions. As a result, the convective thermal resistance in an uncertain convection environment is difficult to obtain from theoretical calculations or manufacturer datasheets. In this paper, the samples of convective thermal resistance are extracted by the thermal network model and the historical working data of the device.

Through time discretization, (1) and (2) are rewritten as

$$\begin{cases} T_{\mathrm{j}}^{k+1} = T_{\mathrm{j}}^{k} + \dfrac{\Delta t}{C_1}\left(P_{\mathrm{loss}}^{k} - \dfrac{T_{\mathrm{j}}^{k} - T_1^{k}}{\theta_1}\right) \\ T_1^{k+1} = T_1^{k} + \dfrac{\Delta t}{C_2}\left(\dfrac{T_{\mathrm{j}}^{k} - T_1^{k}}{\theta_1} - \dfrac{T_1^{k} - T_2^{k}}{\theta_2}\right) \\ \cdots\cdots \\ T_{i-1}^{k+1} = T_{i-1}^{k} + \dfrac{\Delta t}{C_i}\left(\dfrac{T_{i-2}^{k} - T_{i-1}^{k}}{\theta_{i-1}} - \dfrac{T_{i-1}^{k} - T_{\mathrm{c}}^{k}}{\theta_i}\right) \end{cases} \tag{6}$$

$$\begin{cases} T_{\mathrm{c}}^{k+1} = T_{\mathrm{c}}^{k} + \dfrac{\Delta t}{C_{\mathrm{ce}}}\left(\dfrac{T_{m-1}^{k} - T_{\mathrm{c}}^{k}}{\theta_i} - \dfrac{T_{\mathrm{c}}^{k} - T_{\mathrm{e}}^{k}}{\theta_{\mathrm{ce}}}\right) \\ T_{\mathrm{e}}^{k+1} = T_{\mathrm{e}}^{k} + \dfrac{\Delta t}{C_{\mathrm{e}}}\left(\dfrac{T_{c}^{k} - T_{\mathrm{e}}^{k}}{\theta_{ce}} - \dfrac{T_{\mathrm{e}}^{k} - T_{\mathrm{a}}^{k}}{\theta_{e}^{k}}\right) \end{cases} \tag{7}$$

where the superscript k denotes the discrete-time point and Δt represents the discrete step size.

Then, the convective thermal resistance at time k is expressed as

$$\theta_{\mathrm{e}}^{k} = \left(T_{\mathrm{e}}^{k} - T_{\mathrm{a}}^{k}\right)\left[\frac{T_{\mathrm{c}}^{k} - T_{\mathrm{e}}^{k}}{\theta_{\mathrm{ce}}} - C_{\mathrm{e}}\left(\frac{T_{\mathrm{e}}^{k+1} - T_{\mathrm{e}}^{k}}{\Delta t}\right)\right]^{-1} \tag{8}$$

Obviously, the convective thermal resistance θ_e^k can be extracted by using (6) to (8), as long as the heatsink temperature T_e^k, the ambient temperature T_a^k and the device loss P_{loss}^k have been obtained at time k. Then, a sample time series $\left\{\theta_e^k\right\}$ of the convective thermal resistance can be formed with all the extracted results. If the case temperature T_c^k, the heatsink temperature T_e^k and the ambient temperature T_a^k can be measured at the same time, the sample time series $\left\{\theta_e^k\right\}$ can be extracted only by using (8).

3.2. Wavelet Packet Transform and Markov Chain

The time series of the convective thermal resistance is essentially a random process. The airflow in the natural environment has low-frequency and high-frequency changes, therefore the convective thermal resistance also has frequency characteristics. However, the traditional probability density model cannot reflect the randomness of convective thermal resistance in different frequency bands. In this paper, wavelet packet transforms (WPT) and Markov chain (MC), which are widely used scientific methods in the field of signal analysis and processing, are employed to solve this issue.

The WPT is a time-frequency domain signal analysis method, which represents the variation characteristics of signals in different frequency bands by using wavelet packet coefficients [22,23]. The wavelet packet coefficients are obtained by multi-level decomposition of the signal. The decomposition process can be expressed as

$$\begin{cases} w_{l+1}^{2n,r} = \sum_m h_{(m-2r)} w_l^{n,r} \\ w_{l+1}^{2n+1,r} = \sum_m g_{(m-2r)} w_l^{n,r} \end{cases} \tag{9}$$

where $w_l^{n,r}$ is the wavelet packet coefficient. l and n represent the number of decomposition layers and wavelet packet nodes, respectively. m and r are different time points. $h_{(m-2r)}$ and $g_{(m-2r)}$ are the low-pass and high-pass filter coefficients, respectively, which are related to the selected wavelet basis functions.

The signal in the original frequency band can be reconstructed with the wavelet packet coefficients layer by layer. The process of reconstruction can be expressed as

$$w_l^{n,r} = \sum_m \left[\widetilde{h}_{(r-2m)} w_{l+1}^{2n,m} + \widetilde{g}_{(r-2m)} w_{l+1}^{2n+1,m}\right] \tag{10}$$

where $\widetilde{h}_{(r-2m)}$ and $\widetilde{g}_{(r-2m)}$ are the low-pass and high-pass filter coefficients of wavelet packet reconstruction.

The MC is a memoryless stochastic process model which is often used to describe the random changes in ambient wind speed or airflow rate [24–26]. For a Markov process $\{X^k\}$, its state at the time $k+1$ is only related to the state at the time of k. The transition probability p_{ab} from state X^k to state X^{k+1} in the MC can be expressed as

$$p_{ab} = p\left(X^{k+1} = s_b \middle| X^k = s_a\right) \tag{11}$$

where s_a and s_b are the values of states X^k and X^{k+1}, respectively.

If the Markov process has S state values, the transition probabilities between all states can form a matrix $\mathbf{P}$

$$\mathbf{P} = \begin{bmatrix} P_{11} & P_{12} & \cdots & P_{1S} \\ P_{21} & P_{22} & \cdots & P_{2S} \\ \vdots & \vdots & \cdots & \vdots \\ P_{S1} & P_{S2} & \cdots & P_{SS} \end{bmatrix} \tag{12}$$

This matrix is called the state transition probability matrix and describes the statistical characteristics of random transitions between states. After an initial state is given, a

simulated time series with random characteristics similar to the sample series can be generated based on the element values in the matrix **P**.

3.3. Uncertainty Model of Convective Thermal Resistance

The modeling method for the uncertainty of convective thermal resistance is presented in Figure 9. In this method, the sample series of convective thermal resistance $\{\theta_e^k\}$ is decomposed into the wavelet packet coefficients $w_l^{n,r}$ with l-layer wavelet packet decomposition. The randomness of each coefficient is described by a state transition probability matrix $\mathbf{P}_n$ calculated with the Markov chain. Since the wavelet packet coefficients reflect the time-frequency characteristics of the sample series, all the state transition probability matrices form an uncertainty model of the convective thermal resistance series in the time-frequency domain.

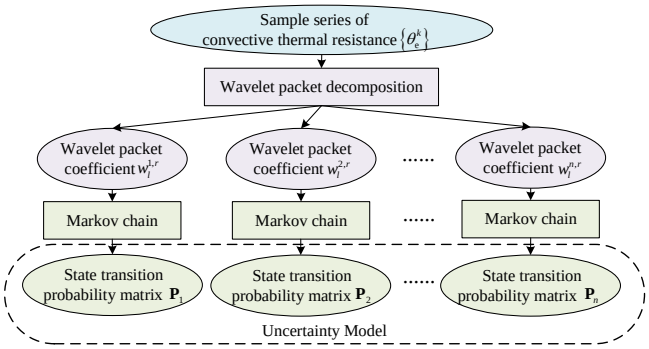


Figure 9. Modeling principle for the uncertainty of convective thermal resistance.

The uncertainty model can be used to simulate the random variations if convective thermal resistance. The specific principle is to randomly simulate the wavelet packet coefficients $w_l^{n,r}$ and to reconstruct all the simulated wavelet packet coefficients $\widetilde{w}_l^{n,r}$, as shown in Figure 10. The random simulation of wavelet packet coefficients depends on the corresponding state transition probability matrix $\mathbf{P}_n$. All wavelet packet coefficients $\widetilde{w}_l^{n,r}$ form a simulation series $\{\widetilde{\theta}_e^k\}$ of convective thermal resistance after wavelet packet reconstruction.

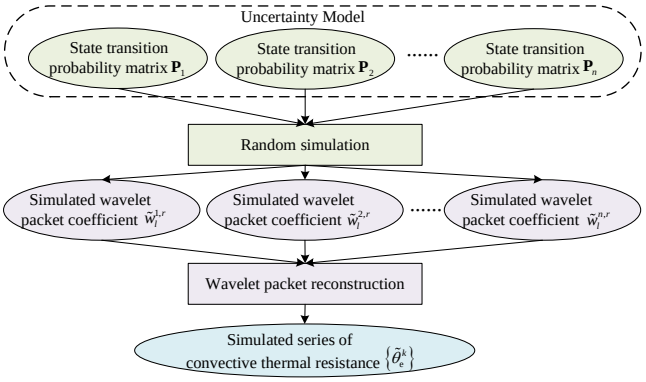


Figure 10. Random simulation of convective thermal resistance based on the uncertainty model.

In the natural environment, the change in airflow is essentially a non-stationary random process. But it can be approximated as a stationary process in a short time (usually a few minutes or tens of minutes). This piecewise stationary assumption is a common method for analyzing non-stationary random signals [27,28]. Since the convective thermal resistance is mainly affected by the airflow, it can also be treated as a piecewise stationary time series. Consequently, the simulated series $\{\widetilde{\theta}_e^k\}$ in a certain period of time can describe the random variations if convective thermal resistance in the next time period.

3.4. Validation Method of the Uncertainty Model

The validity of an uncertain model can be verified by comparing the similarity of the power spectral density (PSD) between the sample time series and the simulated time series. The PSD is a random process analysis method, which reflects the statistical characteristics of the random signal in different frequency bands. Suppose a random process signal is $Y(t)$, its PSD $S_Y(\omega)$ is expressed as [29,30]

$$S_Y(\omega) = \lim_{T\to\infty} \frac{1}{2t_d} E[|F_Y(\omega, t_d)|]^2 \tag{13}$$

where ω is the angular frequency. t_d is the duration of the random signal. $E[\cdot]$ represents stands for statistical averaging operator. $F_Y(\omega, t_d)$ is the Fourier transform of the signal, which is given by

$$F_Y(\omega, t_d) = \int_{-t_d}^{t_d} Y(t) e^{-j\omega t} dt \tag{14}$$

The similarity of PSD can be evaluated by the correlation coefficient method. The closer the correlation coefficient is to 1, the higher the similarity between the compared objects. The closer the correlation coefficient is to 0, the worse the similarity is. Assuming that there are two variables a and b, their correlation coefficient ρ can be defined as [31]

$$\rho = \frac{\mathrm{Cov}(a, b)}{\sqrt{\mathrm{Var}(a)} \cdot \sqrt{\mathrm{Var}(b)}} \tag{15}$$

where $\mathrm{Cov}(a, b)$ is the covariance of a and b. $\mathrm{Var}(a)$ and $\mathrm{Var}(b)$ are the variances of a and b, respectively.

3.5. Validation and Analyses of Uncertainty Model

To verify the validity of the model, the device in the experimental platform works with the rated current I_{rate} and the airflow velocity shown in Figure 7. Figure 11 shows the sample series of the convective thermal resistance extracted with (6) to (8). The extracted results show that the convective thermal resistance always fluctuates randomly under the influence of changing ambient airflow.

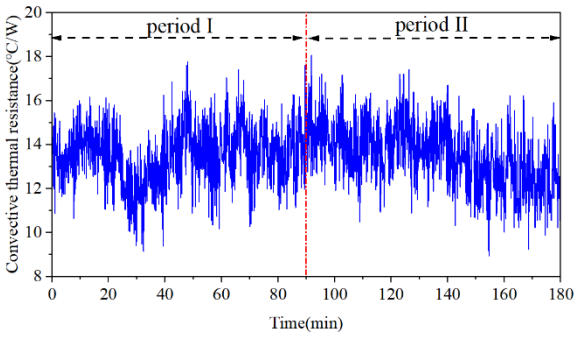
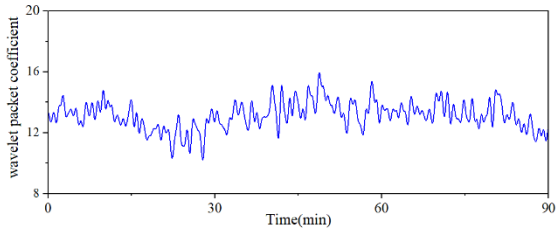


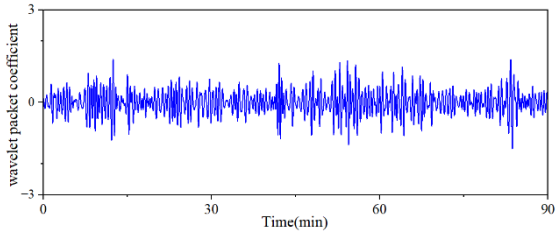
Figure 11. Extracted convective thermal resistance of the device.

The extracted samples in period I and period II are used to establish and validate the uncertainty model of convective thermal resistance, respectively. Figure 12 shows the wavelet packet coefficients decomposed from the convective thermal resistance samples in period I. The wavelet basis function selected in the wavelet packet transform is dB30 wavelet and the decomposition layer is three. Since the sampling rate of the experimental platform is 1 s, the frequency bands decomposed by wavelet packet transform range from 0 Hz to 0.5 Hz. It is easy to find that the fluctuation of the wavelet packet coefficients in sub-frequency band #1 is significantly larger than that in other frequency bands, which

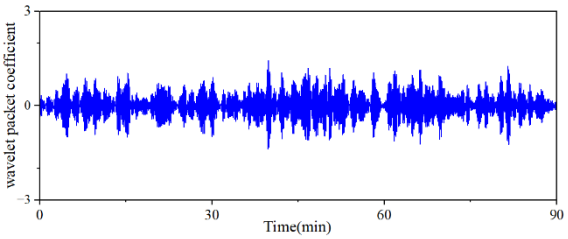
indicates that the random influence of convection on the heat dissipation of the power device is mainly concentrated in the low-frequency band.



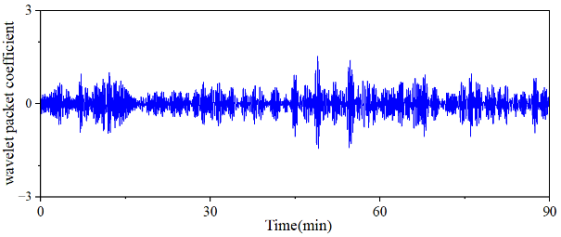
(**a**) Sub-frequency band #1 (0~0.0625 Hz)



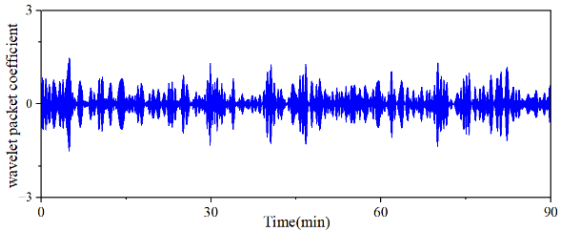
(**b**) Sub-frequency band #2 (0.0625~0.125 Hz)



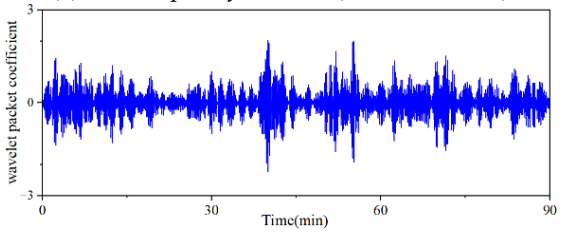
(**c**) Sub-frequency band #3 (0.125~0.1875 Hz)



(**d**) Sub-frequency band #4 (0.1875~0.25 Hz)

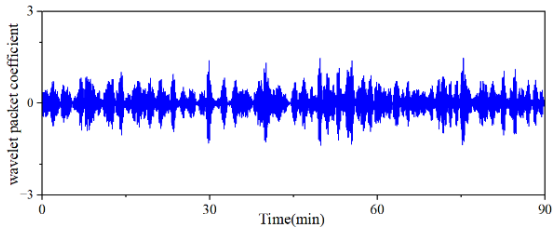


(**e**) Sub-frequency band #4 (0.25~0.3125 Hz)

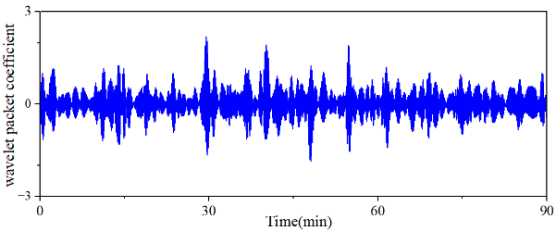


(**f**) Sub-frequency band #5 (0.3125~0.375 Hz)

Figure 12. *Cont*.



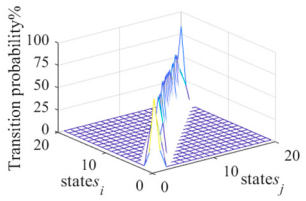
(**g**) Sub-frequency band #6 (0.375~0.4375 Hz)



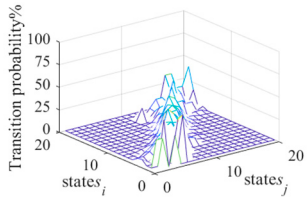
(**h**) Sub-frequency band #7 (0.4375~0.5 Hz)

Figure 12. Wavelet packet coefficients of convective thermal resistance in the time period I.

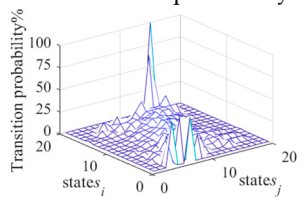
Figure 13 shows the state transition probability of the Markov chain for the different wavelet packet coefficients. In probability statistics, the wavelet packet coefficients in each frequency band are divided into 20 states. The significant difference between the different state transition probabilities verifies the necessity of considering the time-frequency domain characteristics of convective thermal resistance.



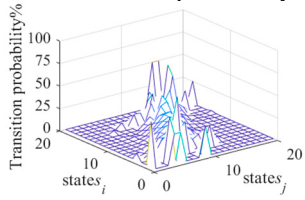
(**a**) State transition probability $\mathbf{P}_1$



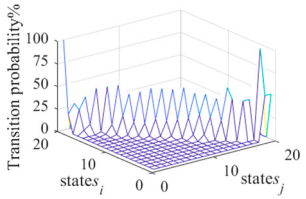
(**b**) State transition probability $\mathbf{P}_2$



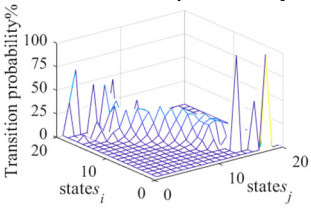
(**c**) State transition probability $\mathbf{P}_3$



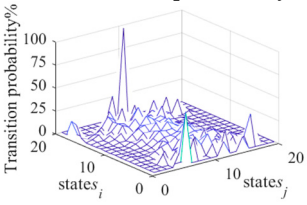
(**d**) State transition probability $\mathbf{P}_4$



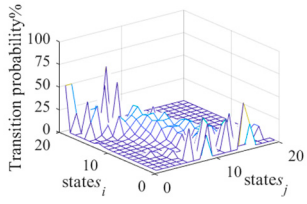
(**e**) State transition probability $\mathbf{P}_5$



(**f**) State transition probability $\mathbf{P}_6$



(**g**) State transition probability $\mathbf{P}_7$



(**h**) State transition probability $\mathbf{P}_8$

Figure 13. State transition probability of Markov chain for the different wavelet packet coefficients.

Based on the above state transition probability, the wavelet packet coefficients can be randomly simulated. The simulated wavelet packet coefficients are reconstructed by wavelet packet to generate a simulated series of convective thermal resistance. Figure 14 shows the PSD of the simulated series and the sample series in period I. To verify the piecewise stationarity of the convective thermal resistance, the PSD of the sample series in period II is also given in this figure. In addition, the similarity between the three PSDs is marked to compare the randomness of different convective thermal resistance series.

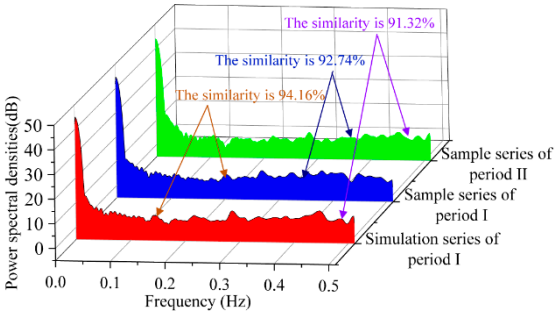


Figure 14. Comparison of the power spectral density between the simulated series and the sample series.

Obviously, the PSD of each series has a higher amplitude in the low-frequency band. This means that the low-frequency component of the convective thermal resistance is very significant, which is consistent with the analysis of wavelet packet transform results. The similarity of PSD between the simulated series and the series in the time period I is more than 90%, which proves that the convective thermal resistance simulated by the proposed uncertainty model has similar random characteristics to the real sample. The similarity of power spectral density between the simulated series and the series in the time period II is also more than 90%, which means the convective thermal resistance sample used in this paper can be regarded as a stationary random series within 30 min. Therefore, the uncertainty model established with the sample of period I can reflect the random characteristics of the convective thermal resistance in the next period.

4. Proposed ATM Method

4.1. Principle of Proposed Method

The principle of the proposed ATM method is shown in Figure 15. In the proposed method, the working current limit I_{lim} is selected by a virtual switch. The control of the switch depends on a logical condition, which is whether the device junction temperature is lower than the maximum allowable value T_{jmax}.

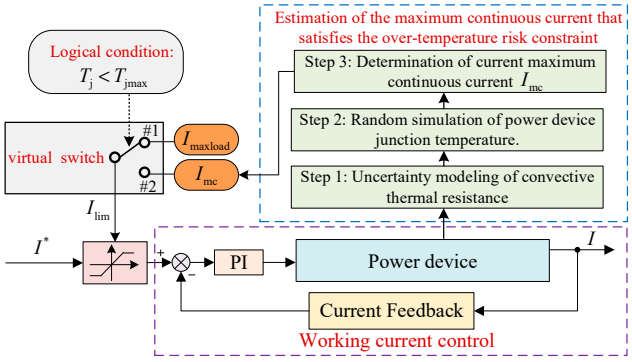


Figure 15. Block diagram of proposed ATM method.

When the logic condition is true, the device meets the thermal safety requirements. This means that the device can work with the maximum load current in a short time regardless of whether the ambient convection changes randomly. Consequently, the switch

is switched to position #1 to select the current I_{maxload} as the current limit I_{lim}. When the logic condition is false, the device can no longer work with the maximum load current, otherwise the random convection may cause the over-temperature of the device. To ensure the thermal safety of the devices, the switch is switched to position #2 to set a current I_{mc} as the current limit I_{lim}. The current I_{mc} is a maximum continuous current of the device that satisfies the over-temperature risk constraint under the random convection conditions. Therefore, the device can continuously work at the current I_{mc} without over-temperature.

The maximum continuous current I_{mc} can be estimated according to the following three steps.

Step 1: Uncertainty modeling of convective thermal resistance. The uncertainty model for the convective thermal resistance of the power device is established by using the method described in Section III. Based on this model, the convective thermal resistance series $\left\{\widetilde{\theta}_{\text{e}}^{k}\right\}$ can be simulated randomly.

Step 2: Random simulation of power device junction temperature. The simulated series of the convective thermal resistance $\left\{\widetilde{\theta}_{\text{e}}^{k}\right\}$ are substituted into the thermal network model to simulate the fluctuation of device junction temperature at the different working current level I_v. If the number of current levels is V and the number of series $\left\{\widetilde{\theta}_{\text{e}}^{k}\right\}$ is H, the number of simulated junction temperature series $\left\{\widetilde{T}_{\text{j}}^{k}\right\}$ is $H \times V$. Theoretically, the greater the values of parameters H and V, the more accurate the random simulation of junction temperature variations. However, in practical engineering, the values of these two parameters need to be comprehensively considered according to the computing power of microprocessors.

Step 3: Determination of the maximum continuous current I_{mc} according to the over-temperature risk of the device. Based on the simulated junction temperature series $\left\{\widetilde{T}_{\text{j}}^{k}\right\}$, the over-temperature probability of the device can be calculated under the different current levels I_v. Then, I_{mc} is set to a maximum current level that satisfies the over-temperature risk constraint condition expressed as

$$P_{\text{r}}\left[\left(\widetilde{T}_{\text{j}}^{k}\middle| I_v|\right) \geq T_{\text{jmax}}\right] \leq P_{\text{rmax}} \tag{16}$$

where $P_{\text{r}}\left[\left(\widetilde{T}_{\text{j}}^{k}\middle| I_v|\right) \geq T_{\text{jmax}}\right]$ is the over-temperature probability under current level I_{v}. P_{rmax} is the maximum allowable over-temperature probability and it should be below 0.5% to ensure that the over-temperature is a small probability event.

Obviously, the basic idea of the proposed model is that when the device junction temperature is lower than T_{jmax}, the short-term current capability of the device is maximized according to the thermal inertia of the device and the maximum load current I_{maxload}. Once the device junction temperature reaches or exceeds T_{jmax}, the continuous current capability of the device is maximized by the maximum current I_{mc} that satisfies the over-temperature risk constraint of the device.

Different from the traditional ATM method, the proposed method does not rely on junction temperature control to maximize the device's current capability. Because of this, the uncertain disturbance of the convection environment to the junction temperature will not cause random fluctuation of the working current. With this feature, the proposed method can safely and stably improve the short-term and continuous current capability of the power device working under random convection conditions.

To avoid repeated switching between the short-term current capability and the continuous current capability, the initial position of the virtual switch should be set at position 1 and can only be switched from position 1 to position 2. This means that the proposed method needs to be reset if the short-term current capacity of the device is to be increased again.

4.2. Verification of Proposed Method

To verify the effectiveness of the proposed ATM method, the power device works in the convection environment with the convective thermal resistance shown in Figure 11. In time periods I and II, the device works with the rated current and the proposed ATM method, respectively. The uncertainty model of the convective thermal resistance established in period I is used in the ATM method in period II. Since this uncertainty model has been presented and verified in Section III, so it is not repeated here.

Based on the principle of the proposed ATM method, the convective thermal resistance of the device is randomly generated by using the uncertainty model, and the simulated convective thermal resistances are used to simulate the random fluctuations of the device junction temperature at different current levels. According to the performance of the microprocessor in this study, the number of convective thermal resistance simulation series and the current levels are selected as 200 and 20, respectively. Then, the over-temperature probability of the device at different currents can be estimated as shown in Figure 16. These probabilities indicate that the maximum continuous current I_{mc} in this experiment should be set to 1.15 pu in order to meet the over-temperature risk constraints of the device.

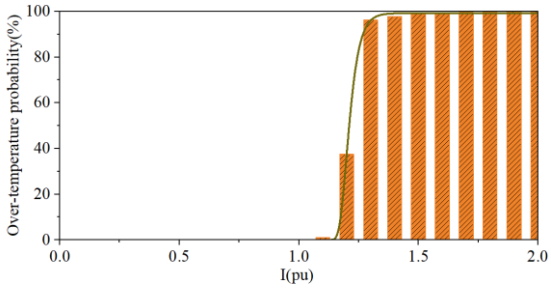


Figure 16. Over-temperature probability of the device at different currents estimated with the proposed ATM method.

After current I_{mc} is determined, the variations if the device junction temperature and working current in the experiment can be analyzed as shown in Figure 17. Similar to the analysis of Figure 8, period II is divided into period III and period IV, corresponding to the stage of improving short-term and continuous current capability of power device, respectively. It is easy to find that the device junction temperatures in period III are lower than T_{jmax}, so the proposed ATM method sets the current limit to the maximum load current. In time period IV, the current limit is set to the maximum continuous current I_{mc}. The junction temperature of the device does not exceed T_{jmax} during the whole period II. Therefore, with the proposed ATM method, the device can work for a short time at 1.2 times the rated current and continuously at 1.15 times the rated current.

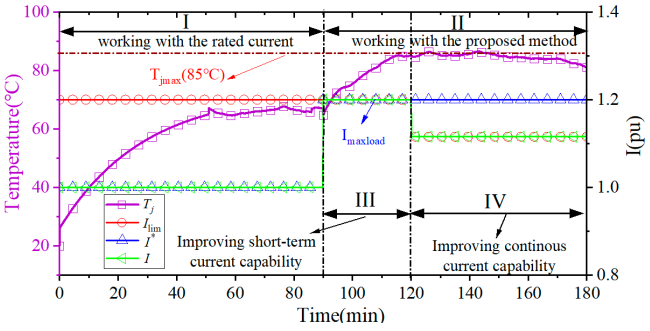


Figure 17. Variations if the device junction temperature and working current in the verification experiment of the proposed method.

To verify the selection rationality of the current I_{mc}, several additional experiments were performed. During the time period IV of these experiments, the power device works

at different current levels. Figure 18 shows the junction temperature change in the device in these experiments. Obviously, the device junction temperature in period IV is much lower than T_{jmax} when the current is less than I_{mc}, which shows that the current capability of the device is not fully improved. On the contrary, when the current in period IV is greater than I_{mc}, the junction temperature exceeds T_{jmax}, which indicates that the current capability is seriously overestimated. When the current in period IV is set to I_{mc}, the fluctuating junction temperature will be close to but never exceeds T_{jmax}. Therefore, the current I_{mc} effectively represents the maximum stable current that satisfies the over-temperature risk constraint.

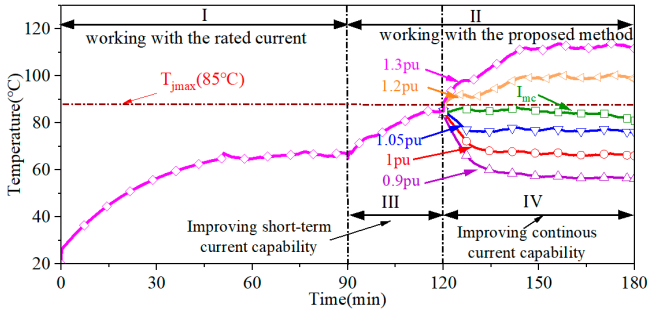


Figure 18. Variations if the device junction temperature in the experiments used to verify the rationality of the current I_{mc} selection.

Based on the above results, it can be found that the proposed method can reliably improve the short-term and continuous current capability of the device under random convection conditions. More importantly, the comparison between Figures 7 and 16 shows that the current capability improved by the proposed method does not fluctuate randomly, which effectively overcomes the shortcomings of the traditional ATM method. Therefore, the proposed method is more suitable for improving the current capability of the power device affected by random convection.

5. Conclusions

A new ATM method is proposed for the power device under random convection conditions. This method maximizes the short-term current capability of the device according to the thermal inertia of the device and maximum load current, which is the same as the traditional method. However, different from the traditional method, the proposed method utilizes a maximum continuous current, which satisfies the over-temperature risk constraint of the device, to maximize the continuous current capacity of the device. To determine the maximum continuous current, an uncertainty model based on wavelet packet transform and Markov chain is proposed for the convective thermal resistance of the power device. With this uncertainty model, the proposed method can safely improve the output performance of the device under random convection conditions without causing random fluctuations in the current capacity. This effectively overcomes the shortcomings of the traditional ATM method, which will lead to uncertain current variations in power devices.

Although the proposed method is only verified on a single-power MOSFET, it lays a foundation for the application of the method in IGBT modules and converters. Therefore, this study provides an important reference for stably improving the overload capacity of IGBT modules and converters under random convection conditions. In future research, the nonlinear junction-to-case thermal resistances will be employed in the proposed method to improve the junction temperature estimation and the device's current capacity more accurately.

Author Contributions: Conceptualization, Y.Z.; Investigation, W.H.; Methodology, W.H., Y.Z. and Z.Y.; Writing—original draft, W.H.; Writing—review and editing, Z.L. and W.Z. All authors have read and agreed to the published version of the manuscript.

Funding: This research was funded by the National Natural Science Foundation of China (Grant No. 42206225) and the Project of State Key Laboratory of Smart Grid Protection and Operation Control (SGNR0000KJJS2007613).

Data Availability Statement: The data is unavailable due to privacy or ethical restrictions.

Conflicts of Interest: The authors declare no conflicts of interest.

References

1. Blaabjerg, F.; Yang, Y.; Kim, K.A.; Rodriguez, J. Power electronics technology for large-scale renewable energy generation. *Proc. IEEE* **2023**, *111*, 335–355. [CrossRef]
2. Fang, J.; Gao, F.; Goetz, S.M. Symmetries in power electronics and lattice converters. *IEEE Trans. Power Electron.* **2022**, *38*, 944–955. [CrossRef]
3. Roj, R.; Katenbrink, N. Investigation on the application of different Air-Cooling-Systems in a thermoelectric Setup. *Mater. Today Proc.* **2015**, *2*, 714–720. [CrossRef]
4. Song, W.; Xu, P.; Chen, J.; Tan, H.; Yang, K.; Tang, T. A Chip Open-Circuit Failure Monitoring Method in Multichip IGBT Modules Based on the Fall Time of Gate-Voltage. *IEEE Trans. Transp. Electrif.* **2024**. [CrossRef]
5. Murdock, D.A.; Torres, J.E.R.; Connors, J.J.; Lorenz, R.D. Active thermal control of power electronic modules. *IEEE Trans. Ind. Appl.* **2006**, *42*, 552–558. [CrossRef]
6. Kuprat, J.; van der Broeck, C.H.; Andresen, M.; Kalker, S.; Liserre, M.; De Doncker, R.W. Research on active thermal control: Actual status and future trends. *IEEE J. Emerg. Sel. Top. Power Electron.* **2021**, *9*, 6494–6506. [CrossRef]
7. Kaczorowski, D.; Michalak, B.; Mertens, A. A novel thermal management algorithm for improved lifetime and overload capabilities of traction converters. In Proceedings of the 17th European Conference on Power Electronics and Applications (EPE'15 ECCE-Europe), Geneva, Switzerland, 8–10 September 2015; pp. 1–10.
8. Lemmens, J.; Driesen, J.; Vanassche, P. Thermal management in traction applications as a constraint optimal control problem. In Proceedings of the 2012 IEEE Vehicle Power and Propulsion Conference, Seoul, Republic of Korea, 9–12 October 2012; pp. 36–41.
9. Polom, T.A.; Wang, B.; Lorenz, R.D. Control of junction temperature and its rate of change at thermal boundaries via precise loss manipulation. *IEEE Trans. Ind. Appl.* **2017**, *53*, 4796–4806. [CrossRef]
10. Wei, L.; McGuire, J.; Lukaszewski, R.A. Analysis of PWM frequency control to improve the lifetime of PWM inverter. *IEEE Trans. Ind. Appl.* **2011**, *47*, 922–929.
11. van der Broeck, C.H.; Ruppert, L.A.; Lorenz, R.D.; De Doncker, R.W. Active thermal cycle reduction of power modules via gate resistance manipulation. In Proceedings of the 2018 IEEE Applied Power Electronics Conference and Exposition (APEC), San Antonio, TX, USA, 4–8 March 2018; pp. 3074–3082.
12. Ko, Y.; Andresen, M.; Buticchi, G.; Liserre, M. Discontinuous-modulation-based active thermal control of power electronic modules in wind farms. *IEEE Trans. Power Electron.* **2018**, *34*, 301–310. [CrossRef]
13. Andresen, M.; Liserre, M. Impact of active thermal management on power electronics design. *Microelectron. Reliab.* **2014**, *54*, 1935–1939. [CrossRef]
14. Sun, T.; Wang, J.; Griffo, A.; Sen, B. Active thermal management for interior permanent magnet synchronous machine (IPMSM) drives based on model predictive control. *IEEE Trans. Ind. Appl.* **2018**, *54*, 4506–4514. [CrossRef]
15. Lemmens, J.; Vanassche, P.; Driesen, J. Optimal control of traction motor drives under electrothermal constraints. *IEEE J. Emerg. Sel. Top. Power Electron.* **2014**, *2*, 249–263. [CrossRef]
16. Andresen, M.; Buticchi, G.; Liserre, M. Thermal stress analysis and MPPT optimization of photovoltaic systems. *IEEE Trans. Ind. Electron.* **2016**, *63*, 4889–4898. [CrossRef]
17. Yu, Y.; Du, X.; Zhou, J.; Ren, H.; Liu, Q.; Luo, Q. Condition Monitoring of Thermal Fatigue of IGBT Module Using Turning Point of Preheating Stage of Case Temperature. *IEEE Trans. Power Electron.* **2022**, *38*, 2866–2871. [CrossRef]
18. Shi, Y.; Liu, J.; Ai, Y.; Chen, S.; Bai, Y. Dynamic IGBT three-dimensional thermal network model considering base solder degradation and thermal coupling between IGBT chips. *IEEE Trans. Transp. Electrif.* **2023**, *9*, 2994–3011. [CrossRef]
19. Yuan, S.; Fu, J.; Cao, D. Dynamic modeling for thermoelectric equipments. In Proceedings of the IEEE International Symposium on Industrial Electronics, Hangzhou, China, 28–31 May 2012; pp. 999–1002.
20. Christen, D.; Biela, J. Analytical switching loss modeling based on datasheet parameters for mosfet s in a half-bridge. *IEEE Trans. Power Electron.* **2018**, *34*, 3700–3710. [CrossRef]
21. Incropera, F.P.; DeWitt, D.P.; Bergman, T.L.; Lavine, A.S. *Fundamentals of Heat and Mass Transfer*; Wiley: New York, NY, USA, 1996.
22. Abari, I.; Hamouda, M.; Sleiman, M.; Slama, J.B.H.; Kanaan, H.Y.; Al-Haddad, K. Open-circuit fault detection and isolation method for five-level PUC inverter based on the wavelet packet transform of the radiated magnetic field. *IEEE Trans. Instrum. Meas.* **2022**, *71*, 3502611. [CrossRef]
23. Chiluveru, S.R.; Raman, B.; Tripathy, M.; Kaushik, B.K. Memory efficient architecture for lifting-based discrete wavelet packet transform. *IEEE Trans. Circuits Syst. II Express Briefs* **2020**, *68*, 1373–1377.
24. Zhong, J.; Liu, J. Assessment on fast simulation of wind-driven pollutant dispersion around a street canyon with regime-switching Markov Chain. *Build. Environ.* **2024**, *258*, 111591. [CrossRef]

25. Li, M.; Yang, M.; Yu, Y.; Lee, W.J. A wind speed correction method based on modified hidden Markov model for enhancing wind power forecast. *IEEE Trans. Ind. Appl.* **2021**, *58*, 656–666. [CrossRef]
26. Li, W.; Jia, X.; Li, X.; Wang, Y.; Lee, J. A Markov model for short term wind speed prediction by integrating the wind acceleration information. *Renew. Energy* **2021**, *164*, 242–253. [CrossRef]
27. Venkataraman, V.; Fan, G.; Havlicek, J.P.; Fan, X.; Zhai, Y.; Yeary, M.B. Adaptive kalman filtering for histogram-based appearance learning in infrared imagery. *IEEE Trans. Image Process.* **2012**, *21*, 4622–4635. [CrossRef] [PubMed]
28. Feng, X.; Liu, C.; Yang, B.; Cui, F.; Li, Q. The extractive method of seismic wavelet in different time window and the application in synthetic seismogram. *Prog. Geophys.* **2002**, *17*, 71–77.
29. Qiu, X.B.; Liu, L.L.; Li, C.L.; Wei, J.L.; Wu, Y.F.; Cui, X.C. Defect classification by pulsed eddy-current technique based on power spectral density analysis combined with wavelet transform. *IEEE Trans. Magn.* **2014**, *50*, 6200708. [CrossRef]
30. Parhi, K.K.; Ayinala, M. Low-complexity Welch power spectral density computation. *IEEE Trans. Circuits Syst. I Regul. Pap.* **2013**, *61*, 172–182. [CrossRef]
31. Otte, M. Elastic registration of fMRI data using Bezier-spline transformations. *IEEE Trans. Med. Imaging* **2001**, *20*, 193–206. [CrossRef] [PubMed]

Disclaimer/Publisher's Note: The statements, opinions and data contained in all publications are solely those of the individual author(s) and contributor(s) and not of MDPI and/or the editor(s). MDPI and/or the editor(s) disclaim responsibility for any injury to people or property resulting from any ideas, methods, instructions or products referred to in the content.